Chaos

# Controlled generation of self-sustained oscillations in complex artificial neural networks

Cite as: Chaos **31**, 113127 (2021); https://doi.org/10.1063/5.0069333
Submitted: 30 August 2021 • Accepted: 20 October 2021 • Published Online: 10 November 2021

**Chang Liu, Jia-Qi Dong, Qing-Jian Chen, et al.**

# Controlled generation of self-sustained oscillations in complex artificial neural networks

Cite as: Chaos **31**, 113127 (2021); doi: 10.1063/5.0069333
Submitted: 30 August 2021 · Accepted: 20 October 2021 ·
Published Online: 10 November 2021



Chang Liu,[1] Jia-Qi Dong,[1,2] Qing-Jian Chen,[3] Zi-Gang Huang,[3,a)] Liang Huang,[1,a)] Hai-Jun Zhou,[2] and Ying-Cheng Lai[4]

## AFFILIATIONS

[1]Lanzhou Center for Theoretical Physics and Key Laboratory of Theoretical Physics of Gansu Province, Lanzhou University, Lanzhou, Gansu 730000, China
[2]CAS Key Laboratory for Theoretical Physics, Institute of Theoretical Physics, Chinese Academy of Sciences, Beijing 100190, China
[3]Key Laboratory of Biomedical Information Engineering of Ministry of Education, Key Laboratory of Neuro-informatics & Rehabilitation Engineering of Ministry of Civil Affairs, and Institute of Health and Rehabilitation Science, School of Life Science and Technology, Xi'an Jiaotong University, Xi'an 710049, China
[4]School of Electrical, Computer and Energy Engineering, Arizona State University, Tempe, Arizona 85287, USA

[a)]**Authors to whom correspondence should be addressed:** huangzg@xjtu.edu.cn and huangl@lzu.edu.cn

## ABSTRACT

Spatially distinct, self-sustained oscillations in artificial neural networks are fundamental to information encoding, storage, and processing in these systems. Here, we develop a method to induce a large variety of self-sustained oscillatory patterns in artificial neural networks and a controlling strategy to switch between different patterns. The basic principle is that, given a complex network, one can find a set of nodes—the minimum feedback vertex set (mFVS), whose removal or inhibition will result in a tree-like network without any loop structure. Reintroducing a few or even a single mFVS node into the tree-like artificial neural network can recover one or a few of the loops and lead to self-sustained oscillation patterns based on these loops. Reactivating various mFVS nodes or their combinations can then generate a large number of distinct neuronal firing patterns with a broad distribution of the oscillation period. When the system is near a critical state, chaos can arise, providing a natural platform for pattern switching with remarkable flexibility. With mFVS guided control, complex networks of artificial neurons can thus be exploited as potential prototypes for local, analog type of processing paradigms.



**Unconventional, non-Boolean systems provide a paradigm for local, analog type of processing such as rapid image or pattern recognition and processing.[1,2] Possible prototypical systems are the oscillatory networks that can generate a large variety of distinct self-sustained periodic oscillations according to needs, which are fundamental to information encoding, storage, and processing in these systems. While exploiting physical systems with engineering design can lead to viable solutions,[3–12] nature has provided us with a rich variety of biological oscillators with dynamical mechanisms leading to operational principles that can be exploited for designing the fundamental oscillator systems.[13–20] Guided by the bio-inspired approach, we investigate artificial neural networks (ANNs) that are capable of generating diverse, stable periodic oscillatory patterns in both space and time. Furthermore, an advantage of using the ANNs is that diverse, distinct oscillation patterns can be generated through control of only a small set of nodes. Intuitively, for an ANN to produce a rich variety of distinct spatiotemporal oscillations, the underlying topology of the network needs to be complex. We are thus motivated to study complex ANNs with the aim to develop an effective method to generate certain self-sustained oscillatory patterns from a given ANN and to uncover the underlying dynamical mechanisms for the emergence, dynamical evolution, and switching of such patterns.**

## I. INTRODUCTION

Complex artificial neural networks (ANNs) belong to the broad class of excitable dynamical systems that arise in many natural processes such as epidemic spreading,[21,22] chemical reactions,[23] spatiotemporal patterns in cardiac tissues,[24] tissue formation,[25,26] and neuronal activities.[27,28] In such a network, the nodes are neurons and the edges represent the electrical or chemical interactions among the neurons. Self-sustained oscillations in neuronal networks play an important role in normal physiological activities[29,30] such as visual perception,[31] cognitive process,[32] olfactory,[33] and arousal and sleep.[34] To maintain sustained oscillations, a network setting is necessary[28,29,35,36] because a single neuron, when isolated, is incapable of exhibiting rich oscillatory behaviors.[37] In excitable media, chaos and transient chaos can also arise.[38,39] In terms of computations, there were previous studies on how memory is encoded, stored, and retrieved in ANNs.[40–43]

What is the basic ingredient required for a complex ANN to generate a rich variety of spatially distinct oscillation patterns? The key lies in the fact that self-sustained oscillations in an excitable system are typically maintained by *loops*. A bi-directional coupled complex network of reasonable size has typically embedded within itself a large number of closed loops that involve different combinations of the nodes in the network.[44–47] In principle, any of the loops can support a self-sustained periodic oscillation pattern in the ANN, i.e., a "pacemaker," with the period being determined by the loop size. While the loops are dense,[44] not all loops can become pacemakers.[48,49] In fact, for a loop to become a pacemaker, the path connecting any two nodes along this loop should be minimum to support a propagating wave. Furthermore, if the length of the loop is too short, it can happen that most of the nodes in the loop would be in a refractory state, breaking the propagation of the excitations along the loop again, leading to a resting state.

Given a network with rich and complex loop structures, how can we induce a self-sustained oscillation pattern of desired length? Our idea is to exploit the minimum feedback vertex set (mFVS)[50–54] to derive a control principle. In particular, for a complex network, an FVS is a subset of nodes (vertices) such that their removal will leave the network with no loop. That is, an FVS is a subset of nodes containing at least one vertex of *every* possible loop in the network. If all FVS nodes are removed, the network will degenerate into a tree or forest structure without any loop, eliminating the possibility of bringing about any self-sustained oscillation. From a different perspective, if some FVS nodes are present, there will then be some loops in the network to support self-sustained oscillations. Typically, FVS is not unique—for a large network, there can be a large number of FVS. A simple way to obtain FVS is randomly removing nodes until no loop exists. This method is equivalent to making a site percolation, and, as a result, removing FVS nodes will destroy the giant connected cluster on which the system functioning relies and break the network into a large number of small disconnected components. However, empirically removing the FVS of the smallest possible size, the minimum FVS (mFVS), to eliminate loops can largely preserve the connectivity of the system. Reintroducing a single or a combination of mFVS nodes into the network will form a particular loop structure and enable it to generate distinct self-sustained oscillation patterns.

In this paper, we study a prototype of complex artificial neural networks and demonstrate that our mFVS based control principle is capable of generating a large variety of distinct self-sustained oscillations in the network. We find that, when all mFVS nodes are suppressed (or inhibited) except for a few or even a single one, various self-sustained oscillation patterns can arise. A dynamical analysis reveals that the system can reach a critical state in the sense of a transition from self-sustained periodic oscillations to chaos. In a critical state, chaos is beneficial because it enables the system to be remarkably flexible in the sense that it can quickly switch from one oscillation pattern to another spatially distinct one through an alteration of the active mFVS node. The maintained mFVS nodes leading to specific self-sustained oscillating patterns are effectively memory triggers for the respective patterns to be recalled and realized. Critical phenomena with implications to memory encoding, storage, and retrieval are studied. Our findings suggest that complex artificial neural networks incorporating mFVS guided control can be exploited to efficiently generate and switch self-sustained oscillation patterns.

We note that the concept of FVS has been exploited[55,56] previously for controlling networks of nonlinear oscillators with strong dissipation, where such a network can be fully controlled if all nodes in an FVS are directly driven by external inputs. Particularly, when the FVS nodes have been controlled, the effect of control will "propagate" to all other nodes in the network, driving the whole network to a desired state. For example, if the target state is a limit cycle, insofar as the dynamical variables of the FVS nodes are "pinned" to the corresponding set of the cycle, the whole network will converge to it. It was established mathematically[55,56] that, for nodal dynamical processes described by a set of nonlinear differential equations with dissipation, harnessing properly the dynamical variables of the FVS nodes can bring the whole system to a desired state. Our problem is different as there is no target state, and we seek to generate as many distinct and desired self-sustained oscillation patterns as possible and efficient switching strategy between different patterns for a given ANN with minimum control.

## II. MODELS

Given a complex network, the problem of finding the mFVS is an NP-hard problem. Nonetheless, for networks of a reasonably large size, an effective numerical method has been developed based on the belief propagation algorithm.[50] Here, we consider a random regular network, whose nodes have the same degree $k$, i.e., the number of edges, that are randomly connected between different nodes. An example of the mFVS of a random regular network of size $N = 200$ and degree $k = 3$ is shown in Fig. 1(a), where there are 51 nodes in the mFVS (marked by the gray open squares). When the mFVS is removed or inhibited, the remaining nodes in the network constitute two tree-like components with one connected tree containing almost all the nodes. This intrinsic connectivity is a virtue of the mFVS method because, if one tries to eliminate loops in a network through the traditional site-percolation method, a much larger number of nodes will need to be removed and the resulting network will be fragmented.

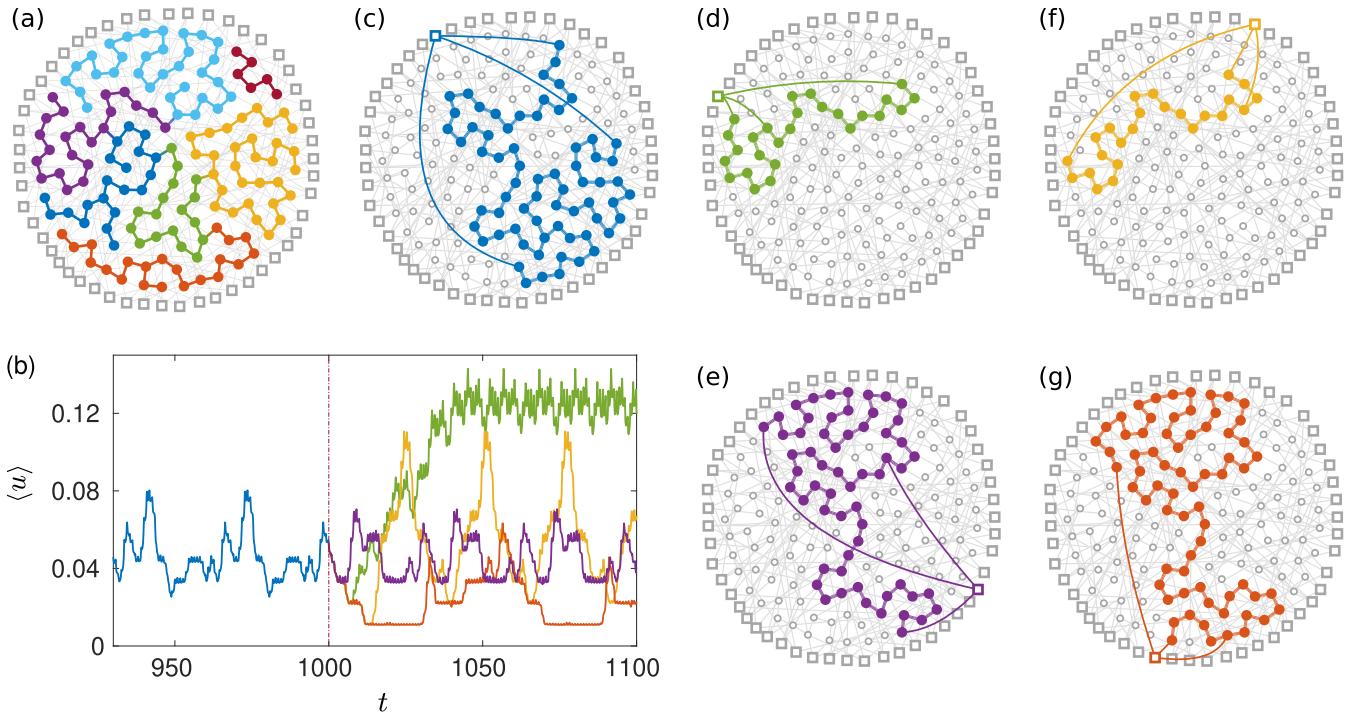


**FIG. 1.** Example of mFVS and illustration of the generation of different attractors with spatially distinct self-sustained oscillation patterns. As different mFVS nodes are excited, the network generates distinct attractors. (a) A random regular network of size $N = 200$, where the mFVS consists of 51 nodes (denoted by the gray open squares on the periphery). When the mFVS is removed or inhibited, the remaining nodes form a tree-like network, as highlighted by the colored filled circles. Numerically, setting the value of the coupling parameter $D_i$ of an mFVS node to a small value will inhibit it, while a proper finite value will activate it. (b) When different mFVS nodes [colored open squares in (c)–(g)] are stimulated, the network can generate different attractors. (c) The loop structure of the attractor generated in the time interval $t < 1000$ by setting the coupling parameter of a specific mFVS node (blue open square) to 0.4 while keeping those for all other mFVS nodes at a lower value, e.g., $D = 0.08 < D_c$, to ensure that these nodes are suppressed. (d)–(g) Attractors with distinct loop structures generated by activating different mFVS nodes (the green, purple, yellow, and red open squares, respectively) for $t \geq 1000$. In principle, activating some mFVS nodes or combinations of these nodes can result in a large number of self-sustained, spatially distinct oscillation patterns.

We consider a class of excitable networked systems,[57] a generalized version of the piece-wise linearized FitzHugh–Nagumo (FHN) neural network model,[37,58] where the nonlinear elements are a simplified version of the Hodgkin–Huxley (HH) type of neurons.[59] We will mainly focus on the FHN system to demonstrate the working of our scheme and then verify with the HH system that our results are general and not depend on specific models. In the main text, we shall only consider the random regular network of size $N = 200$ and degree $k = 3$ as an example to demonstrate the working of the mFVS based control. Consistent results of different network models are presented in Appendix A, and the efficiency of the mFVS based controlling scheme in larger systems is demonstrated in Appendix B.

### A. Model of FitzHugh–Nagumo type of ANNs

Mathematically, the FHN system is described by

$$\frac{du_i}{dt} = -\frac{1}{\epsilon}u_i(u_i - 1)\left(u_i - \frac{v_i + b}{a}\right) + D_i\Sigma_i,$$

$$\frac{dv_i}{dt} = f(u_i) - v_i,\ i = 1, \ldots, N, \tag{1}$$

$$f(u_i) = \begin{cases} 0, & u_i < 1/3, \\ 1 - 6.75u_i(u_i - 1)^2, & 1/3 \leq u_i \leq 1, \\ 1, & u_i > 1, \end{cases}$$

where $u_i$ is the membrane potential of neuron $i$, $v_i$ is a dynamical variable characterizing the collective effect of the underlying ionic channels, $D_i$ is the coupling parameter, and $\Sigma_i$ is the coupling term characterizing the influences of other neurons on the dynamics of neuron $i$. Typical parameter values are $a = 0.84$, $b = 0.07$, and $\varepsilon = 0.04$. A neuron in the network is connected with other neurons through electrical synapses modeled by

$$\Sigma_i = \frac{\sum_j A_{ij}u_j}{\sum_j A_{ij}u_j + K} - u_i, \tag{2}$$

where $A_{ij}$ is an element of the adjacency matrix of the network and $K = 0.8$. For a concrete example, we assume that the neural network has the random regular topology with 200 nodes and 300 edges. For

a non-mFVS node, we set the value of its coupling parameter to be $D_i = 0.4$. The parameter setting is such that a resting node can be excited by a single spike from a neighboring node. For clarity, we reserve $D$ to denote the coupling parameter associated with all the mFVS nodes (except the activated one).

In our simulations, the initial values of $u_i$ and $v_i$ are randomly chosen from the unit interval $[0, 1]$. For typical initial condition, the networked system evolves toward some stable, biologically meaningful state, e.g., a self-sustained oscillatory state. For example, for $D = 0.4$, we find that the probability for the system to exhibit self-sustained oscillations is approximately 97%.

### B. Model of Hodgkin–Huxley type of ANNs

The Hodgkin–Huxley (HH) equations of a single neuron $i$ are

$$C\frac{dV_i}{dt} = -g_{Na}m_i^3h_i(V_i - E_{Na}) - g_K n_i^4(V_i - E_K) - g_L(V_i - E_L) + I_i^{syn}, \quad (3)$$

where $V_i$ is the membrane potential, $C = 1\,\mu F/cm^2$ is the membrane capacitance, $g_{Na} = 120\,mS/cm^2$, $g_K = 36\,mS/cm^2$, and $g_L = 0.3\,mS/cm^2$ are the maximum conductivity of the sodium ion, the potassium ion, and the leak channels, respectively. The Nernst potentials are $E_{Na} = 115\,mV$, $E_K = -12\,mV$, and $E_L = 10.6\,mV$. The gating variables $m$ and $h$ are associated with the activated and inactivated channels of sodium, respectively, and the variable $n$ is for the activated channels of potassium. The differential equations describing the evolution of the gating variables are

$$\frac{dx_i}{dt} = \alpha_{x_i}(V_i)(1 - x_i) - \beta_{x_i}(V_i)x_i, \quad x_i = m_i, h_i, n_i, \quad (4)$$

where $\alpha_{x_i}$ and $\beta_{x_i}$ are given by[60]

$$\alpha_{m_i} = 0.1\frac{25}{\exp[(25 - V_i)/10] - 1}, \quad \beta_{m_i} = 4\exp(-V_i/10),$$

$$\alpha_{n_i} = 0.01\frac{(10 - V_i)}{\exp[(10 - V_i)/10] - 1}, \quad \beta_{n_i} = 0.125\exp(-V_i/80),$$

$$\alpha_{h_i} = 0.07\exp(-V_i/20), \quad \beta_{h_i} = \frac{1}{\exp[(30 - V_i)/10] + 1}.$$

The interaction between neurons is through the current $I_i^{syn}$ given by

$$I_i^{syn} = \sum_j DA_{ij}(V_i - V_j), \quad (5)$$

where $A_{ij}$ is the $ij$th element of the adjacency matrix and $D$ is the coupling strength.

## III. RESULTS

### A. Self-sustained oscillation patterns, chaos, and control in FitzHugh–Nagumo neural networks

We first study FitzHugh–Nagumo (FHN) type[37,58] of ANNs. In general, self-sustained oscillations result from the spreading or propagation of excitation along selective, spatially distinct loops. For a sizable network of neurons, the number of distinct loops can be large and tends to increase exponentially with the network size.[49] Some loops can act as *pacemakers* and lead to self-sustained oscillations at the scale of the whole system. Once such a loop has emerged, it dominates the system dynamics as the neural activities of the nodes not keeping pace with the loop are greatly suppressed. Any loop must necessarily contain at least one mFVS node. Activating a different mFVS node can result in a spatially distinct oscillation pattern associated with a different attractor of the system, as exemplified in Fig. 1(b). Figures 1(c)–1(g) show the spatial structures of five different loops (colored nodes and links) generated by activating five different mFVS nodes (colored open squares), respectively, each corresponding to a spatially distinct pattern of self-sustained oscillations.

In addition to self-sustained oscillation patterns, rich spatiotemporal dynamical behaviors can emerge in system (1) through manipulation of the mFVS nodes, e.g., through a change in the value of their associated coupling parameter. For the parameter setting in Fig. 1, when the coupling parameter is set to be $D = 0.4$ for all mFVS nodes, the ensemble averaged membrane potential $\langle u(t)\rangle \equiv \sum_i u_i(t)/N$ exhibits periodic oscillations of relatively large amplitude. As the value of $D$ for all the mFVS nodes is decreased, a transition in the system dynamics from periodic to chaotic oscillations can occur. If $D$ decreases further and passes a critical value $D_c$, no oscillatory state exists in network dynamics. Note that in general, $D_c$ depends on the neuron model and also the network model. For the FHN system on random regular networks of size $N = 200$ and $k = 3$, through scanning the value of $D$ with a step of 0.001, it is found that $D_c \cong 0.096$. In particular, Fig. 2(a) shows that, for $D = 0.1$, a small perturbation $\boldsymbol{\delta} \to 0$ upon the potential $\boldsymbol{u}$: $\boldsymbol{u}^*(0) = \boldsymbol{u}(0) + \boldsymbol{\delta}$ leads to a new orbit $\boldsymbol{u}^*(t)$ that separates exponentially from the original orbit $\boldsymbol{u}(t)$,

$$\|\Delta\| = \|\boldsymbol{u}^*(t) - \boldsymbol{u}(t)\| \sim \|\boldsymbol{\delta}\|\exp(\lambda t), \quad (6)$$

where $\lambda$ is the maximum Lyapunov exponent. In a chaotic state, the separation $\|\Delta\|$ will reach a certain value, e.g., $10^{-3}$, at time $\tau$. Figure 2(b) shows that $\tau$ decreases logarithmically with the perturbation magnitude $\|\delta\|$, and the slope of the fitted line is approximately $-1/\lambda$. In particular, we have $\lambda = 0.121$ for $D = 0.099$ and $\lambda = 0.0962$ for $D = 0.14$. Figure 2(c) shows the localization measure, the inverse participation ratio $L$ of the power spectrum $S(T)$ of $\langle u(t)\rangle$ defined as

$$L = \sum_T S^4(T) \Big/ \left(\sum_T S^2(T)\right)^2 \quad (7)$$

vs $D$, where

$$S(T) = \left|\int \langle u(t)\rangle\, e^{it/T}\, dt\right|^2.$$

Due to the loop structure, $S(T)$ typically contains separate peaks. If $S(T)$ has one or two dominant peaks, the value of $L$ is large. In contrast, if there is chaos so that $S(T)$ is broad, the value of $L$ is small. Relatively small values of $L$ are thus indicative of chaos. As $D$ decreases from about 0.1, the weak coupling leads to isolation of the mFVS nodes from the system, ruling out self-sustained oscillations. Note that all the mFVS nodes are inhibited. If in this process, one particular mFVS node stays activated, for $D < 0.1$, only the loop

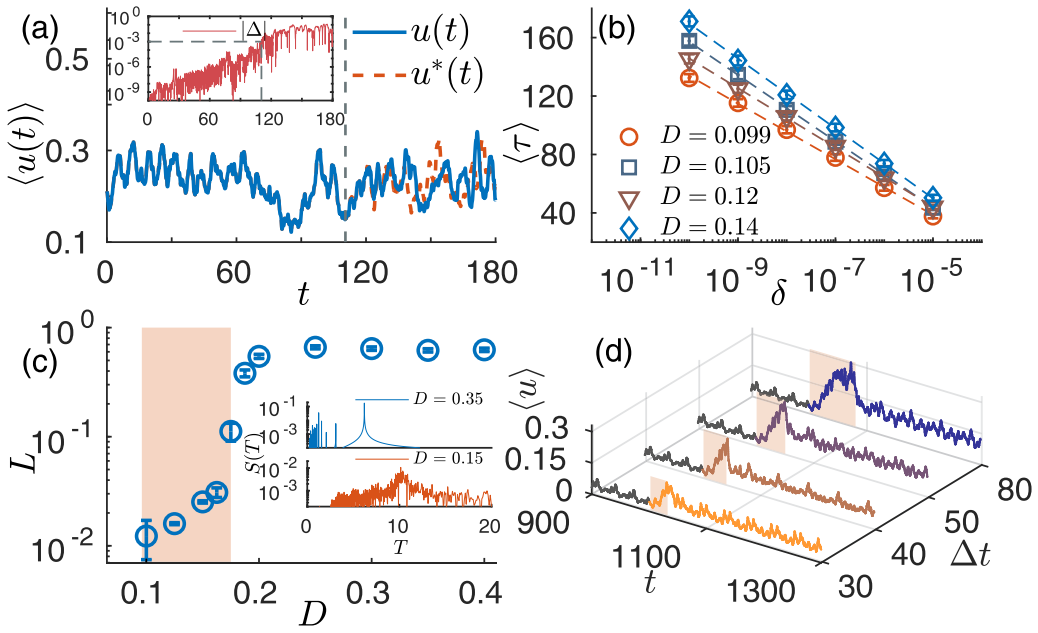


**FIG. 2.** Induced chaotic behavior in the ANN. A chaotic attractor emerges when all mFVS nodes are inhibited properly. (a) Demonstration of sensitive dependence on initial conditions: exponential separation of two trajectories of $\langle u(t)\rangle$ due to an initial perturbation of magnitude $|\delta| = 10^{-10}$, where $D = 0.1$ for all the mFVS nodes and $D_i = 0.4$ for all the other nodes. (b) For $\Delta = 10^{-3}$, the average time $\langle\tau\rangle$ for the differences between the two initially nearby trajectories to reach $\Delta$ vs the initial perturbatio $\delta$. Each data point is the result of averaging 100 realizations. (c) The inverse participation ratio $L$ of the power spectrum $S(T)$ of $\langle u(t)\rangle$ vs $D$. In the shaded region $0.096 < D < 0.175$ where chaos arises, the resulting oscillatory behavior is the consequence of the interactions among a number of pacemakers. Each data point corresponds to the average of 100 random realizations with different sets of initial values $\{u_i(0), v_i(0),\ i = 1, \ldots, N\}$ sampling from the unit interval [0, 1]. (d) Chaos enabled switching among different self-sustained oscillation patterns. As the value of $D$ of the coupling of all the mFVS nodes except the activated one increases from 0.08 to 0.092 at $t = 1000$, a transition in the system dynamics from a periodic to chaotic attractor (the shaded region) occurs. After a time $\Delta t$, $D$ returns to the original value 0.08 and the system approaches a different periodic attractor, which also depends on the interval $\Delta t$.

induced by this mFVS node exists and supports self-sustained oscillations, as shown in Fig. 1. In this case, $L$ takes on a large value again (see Figs. 7–9 in Appendix A).

That chaos can arise when all the mFVS nodes are inhibited can be advantageous for switching the system dynamics from one sustained oscillation to another. In particular, as the mFVS nodes are gradually inhibited (accomplished by a continuous decrease in the value of the coupling parameter $D$ from a relatively large value), transition in the system dynamics from large amplitude periodic oscillations to chaos occurs. The propagation patterns along different loops mix with each other in a complex way, making it difficult to recognize a loop as a "pacemaker." The chaotic oscillations can typically sustain for a relatively long time. At the transition point, the system possesses effectively a tree-like structure with no active loop. At this time, turning on any individual mFVS node by increasing its $D_i$ value significantly can lead to self-sustained oscillations generated by the loop due to this mFVS node. Activating different mFVS nodes can lead to spatially distinct oscillation patterns. Qualitatively, this behavior is similar to that arising in controlling chaos:[61–63] chaos offers a natural platform for switching to stabilizing different unstable periodic orbits at different time points.

Figure 2(d) demonstrates the attractor switching behavior through activation of the originally inhibited mFVS nodes. Here, initially, the system has only one mFVS node activated with $D_i = 0.4$, while all the other mFVS nodes are inhibited by setting their coupling to $D = 0.08$. The system evolves to a self-sustained oscillation pattern for $t < 950$. As the value of $D$ of all the inhibited mFVS nodes (except for the excitable one) increases from 0.08 to 0.092, the system evolves into a chaotic state, as revealed by the shaded region in Fig. 2(d). After a time $\Delta t$, we tune back the $D$ value to 0.08. The system converges to a different periodic attractor, although $D_i$s recover to the same profile. In fact, modulating the length of $\Delta t$ results in different periodic attractors and hence different self-sustained oscillation patterns.

To better understand the mechanism behind the generation of spatially distinct self-sustained oscillations through controlled activation of mFVS nodes, we consider the simple case in which a single mFVS node (denoted by $m$) is excitable, while all the remaining mFVS nodes are inhibited. The node, being part of mFVS, may simultaneously belong to a number of loops in the network, and, hence, activating the node makes it feasible to generate a number of distinct self-sustained, periodic oscillation patterns, as exemplified in Fig. 1. The number of loops that this mFVS node can induce to the tree-like network is less than or equal to $k(k-1)/2$, where $k$ is the degree of this node. Among these loops, typically, one acts as a pacemaker that drives the other loops and hence the whole system.

Depending on the initial condition, the pacemaker can be different, either supported by a different loop activated by the same mFVS node or the same loop but with a different propagation direction. Figure 3 displays the patterns of $\langle u(t)\rangle$ and the corresponding topological structure of the network with a single mFVS node activated (the blue open square), where multiple patterns can be seen. The reasons for a single mFVS node to stimulate multiple self-sustained oscillation patterns are twofold: (1) among all the loops that contain $m$, more than one can act as a pacemaker depending on initial states, and (2) there can be multiple routes to stimulating even a single pacemaker. The two distinct patterns in Figs. 3(a) and 3(b) correspond to the clockwise and counterclockwise stimulation processes for a given loop, as illustrated by the filled blue circles shown in Figs. 3(c) and 3(d), the respective snapshots of the firing neurons. Figure 3(e) shows the normalized power spectrum of $\langle u(t)\rangle$ obtained from different realizations, where the gray solid trace is the average and the dotted curves indicate the power spectra of three spatially distinct self-sustained oscillation patterns. The mFVS node $m$ induces three loops, and the components contributed by the three loops as a pacemaker can be identified in the power spectra. Particularly, the insets show the cases with three different colored loops playing the role of a pacemaker, and the corresponding peaks in the power spectra are marked by the same color.

The features revealed by the power spectra in Fig. 3(e) and the underlying topological loop features imply that an arbitrary dynamical pattern of a complex artificial neural network can be regarded

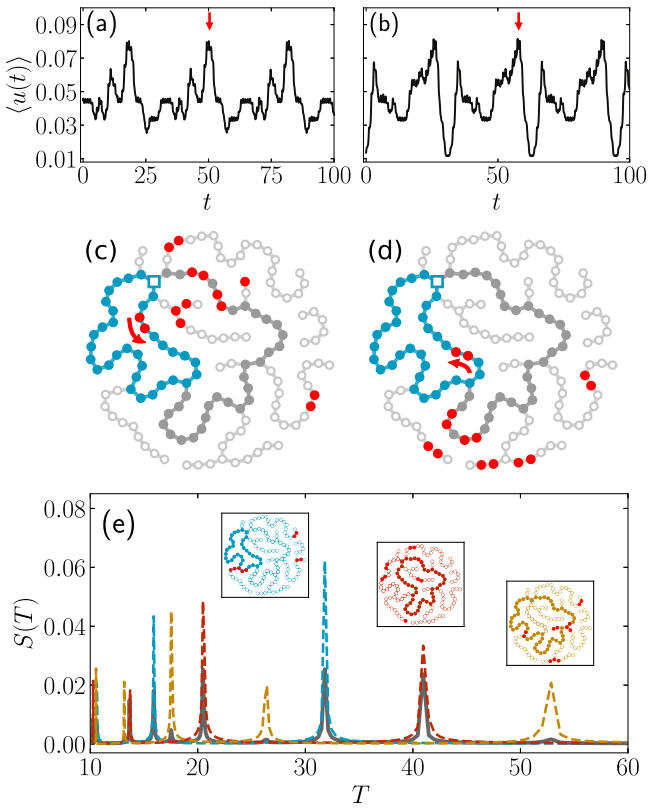


**FIG. 3.** Multiple attractors belonging to one given configuration in controlling mFVS. Shown is a case where one given mFVS node $m$ is excitable (with $D_m = 0.4$, the blue open square) and all other mFVS nodes are inhibited (with $D = 0.08$, not shown). (a) and (b) As the active mFVS node $m$ can belong to different loops, multiple coexisting attractors can arise, generating spatially distinct self-sustained oscillation patterns revealed by the time evolution of $\langle u(t)\rangle$. (c) and (d) The corresponding snapshots of the oscillation patterns in (a) and (b), respectively, at the time indicated by the red arrow, and the firing nodes are red colored. The arrow indicates the propagation direction of the firing dynamics. (e) Normalized power spectrum of $\langle u(t)\rangle$ from different realizations. The thick gray curve denotes the mean power spectrum averaged over a few hundred realizations.

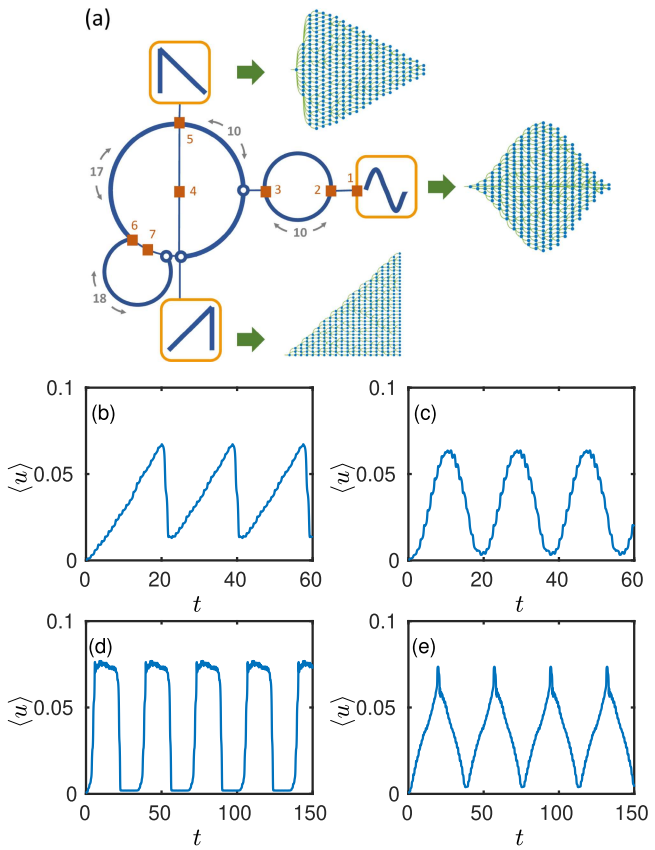


**FIG. 4.** Representative waveform that can be generated through controlled activation of mFVS nodes. (a) A schematic diagram of the network structure. The red squares are possible mFVS nodes, and a blue hollow circle indicates a single node. The thick blue lines are one dimensional chains of artificial neurons with length marked by gray numbers. The thin lines are connections between two artificial neurons. The orange rectangles are three waveform generators, with the detailed artificial neuron connections shown on their right side. Besides the waveform generator of sinusoidal function, other two generators are tree-like structures. An mFVS of this network contains four nodes, but the selection is not unique. Some examples of mFVS are {1, 2, 4, 6} or {1, 2, 5, 7}. Through controlling mFVS, different wave patterns can be generated: (b) a sawtooth wave (with nodes 1, 2, and 5 inhibited), (c) a sinusoidal wave (with nodes 2, 5, and 7 inhibited), (d) a square wave (with nodes 1, 2, and 7 inhibited), and (e) a triangular wave (with nodes 1, 2, and 4 inhibited).

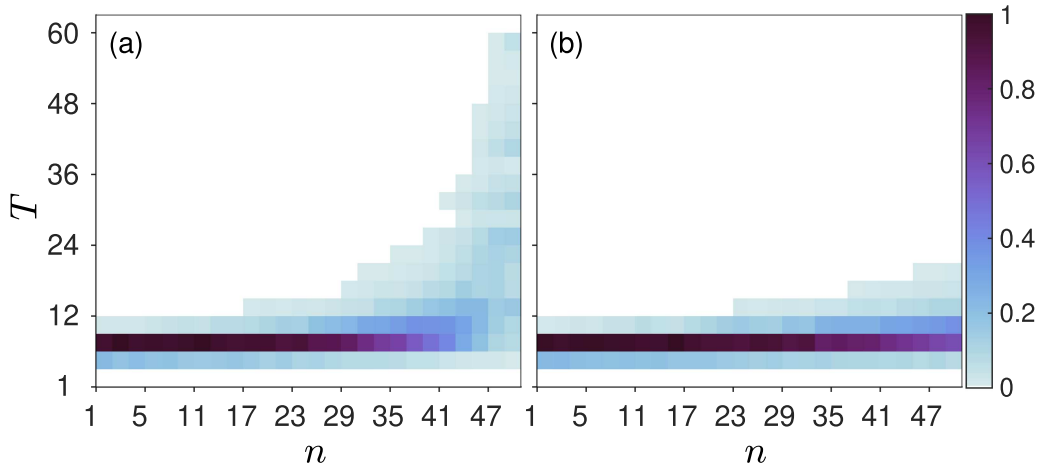


**FIG. 5.** Statistical distribution of the periods of self-sustained oscillations with targeted mFVS based control (a) and random control (b). Ten network realizations with 51 nodes in mFVS are used for obtaining the statistics. For each realization, $n$ nodes randomly selected from an mFVS or from the whole system are inhibited, corresponding to targeted mFVS based control and random control, respectively. Inhibition is implemented by reducing the coupling strength of the controlled nodes to a small value (e.g., 0.08) from the normal value (0.4). If the network produces periodic oscillations, the value of the period ($T$) is recorded. Examining a large number of random nodal sets across all ten network realizations enables the distribution of the periods to be calculated. The distribution corresponding to targeted control is shown via a colored heat-map in (a), whereas the periods resulting from random control are shown in (b) with a much narrower range. Random control results in oscillation patterns of short periods, while the mFVS based targeted control results in a much broader distribution of the periods.

as the superposition of the basic components of pacemakers. This may have potential applications in unconventional computing: various collective oscillatory patterns with a desired waveform can be generated through a proper combination of the mFVS nodes and thus the corresponding pacemakers. This is demonstrated in Fig. 4, where a number of representative waveform that can be generated through pacemakers from mFVS based control are shown: (b) a sawtooth wave, (c) a sinusoidal wave, (d) a square wave, and (e) a triangular wave. Through controlled activation of as few as a single mFVS node, a complex ANN can generate various types of waveform through combining modes distributed in the networks. This might provide useful guidelines for designing artificial neural network hardware.

Finally, we demonstrate that our mFVS based control strategy can lead to a wide variety of distinct self-sustained oscillations. Figure 5 presents the statistical distribution of the periods of the resulting periodic oscillations from two scenarios: (a) targeting mFVS and (b) controlling a random set of nodes. Specifically, for scenario (a), the inhibited nodes are randomly selected from an mFVS with the number of the inhibited nodes less than its size (51), and, for scenario (b), we inhibit a randomly chosen set of nodes, whose number is denoted as $n$. For example, for the network in Fig. 1, an mFVS contains 51 nodes. We carry out a statistical test where, for each realization, we inhibit $n$ ($n \leq 50$) randomly chosen nodes [from an mFVS for (a) and from the whole system for (b)] and calculate the periods of the resulting self-sustained oscillations (if they occur). Nodal inhibition is accomplished by reducing the coupling parameter value from 0.4 to a small value (e.g., 0.08). The left column of Fig. 5 displays a distribution of the periods of the self-sustained oscillations from many realizations following scenario (a). For scenario (b), the distribution of the period of the self-sustained oscillation patterns concentrates in a much smaller range with relatively small periods. This means that inhibiting a random set of nodes is unable to efficiently eliminate the loops, and consequently, a large number of short loops exist in the network, leading to self-sustained oscillations of small periods. This can also be seen from the localization of the power spectrum in Fig. 2(c), where the oscillation periods of the unperturbed network are distributed in a region of small periods. In contrast, when most mFVS nodes are inhibited (e.g., by setting the values of the coupling parameters for all the mFVS nodes to 0.08 except for the excitable one whose coupling strength is 0.4), the resulting distribution of the oscillation period becomes much broader, as shown in Fig. 5(a). Targeted control of the mFVS can thus generate a broad spectrum of self-sustained oscillations with significantly longer periods than those that can be naturally generated in the uncontrolled network.

Our extensive numerical computations with the FHN neural networks reveal that loops capable of hosting self-sustained oscillations can act as pacemakers through controlled activation of mFVS nodes. These nodes thus provide a powerful platform to control the dynamics of complex artificial neural networks. Controlled activation of proper sets of mFVS nodes can induce a large number of distinct pacemakers, greatly enriching the dynamical outcomes and enhancing the expression ability of the networked system.

### B. Self-sustained oscillations and chaos in Hodgkin–Huxley neural networks

To demonstrate the generality of the correspondence between the loop structure in ANNs and self-sustained oscillations, we further exploit the full Hodgkin–Huxley (HH) type of ANNs. In fact, the two-dimensional FHN neuron model is a simplification of the

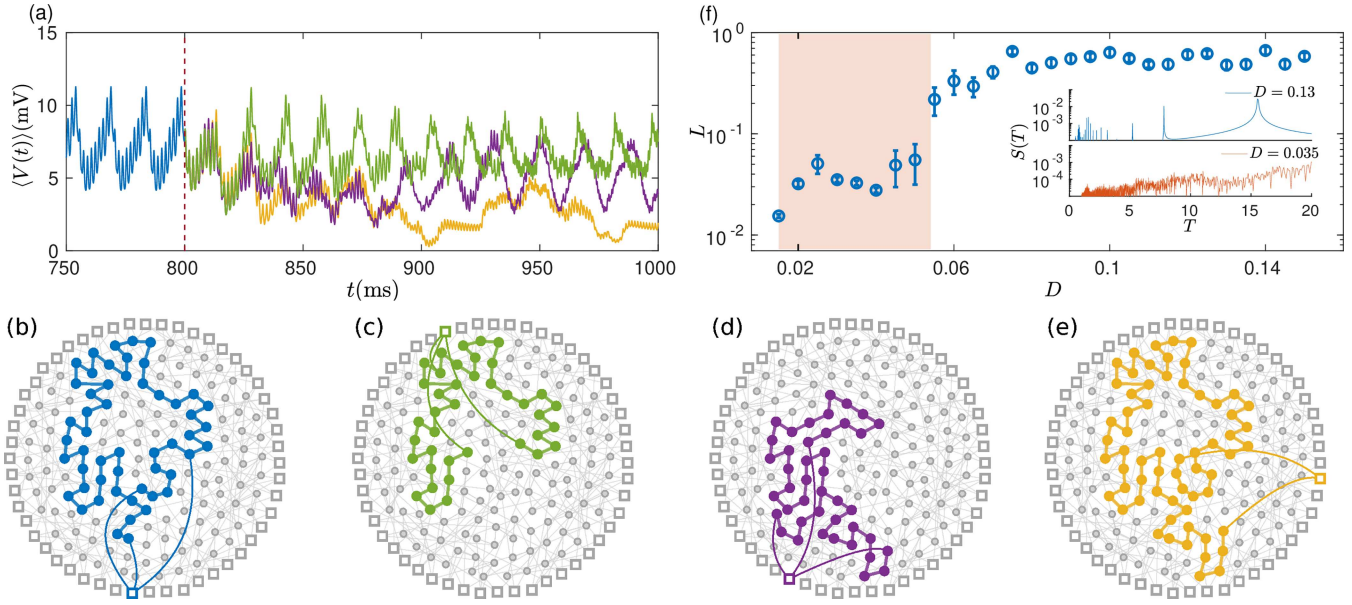


**FIG. 6.** Self-sustained oscillations and switching behavior in the HH network. The network topology is of the regular random type with $N = 200$ nodes and degree $k = 3$. (a) Switching among distinct oscillation patterns. For $t < 800$ ms, the HH system is dominated by a loop activated by the blue square node in (b). At $t = 800$ ms, this node is inhibited, and a different node in the mFVS is excited, activating a different loop. The dynamics of the HH system approach different attractors after a transient. (c)–(e) The spatial configurations of three loops that generate distinct self-sustained oscillation patterns, as indicated in (a) for $t > 800$ ms. Each configuration contains a distinct subset of excitable nodes. (f) Shown is the inverse participation ratio $L$ of the power spectrum of the self-sustained oscillations vs $D$, the coupling strength of all mFVS nodes. The shaded region corresponds to chaotic oscillations that can be exploited to switch between different attractors via transient chaos. Each data point is an average over 50 random realizations.

HH quaternion neuron equation of a giant axon of squid.[59] The HH model better describes the experimentally observed firing behaviors of neurons, as the model captures the change not only in the membrane potential but also in the gated ion channels at a detailed level. To demonstrate the generality of the above results, we investigate coupled HH neurons on a regular random network.

Since the refractory period of the HH neuron is longer than that of the FHN neuron, a large number of random initial conditions are needed to realize self-sustained oscillations (e.g., about one in every 1000 initial conditions). We articulate an initialization procedure to overcome this difficulty. In particular, initially, we set all nodes to the resting state and randomly excite one neuron and inhibits its two neighbors for a short period of time. While this initialization does not lead to all possible states of periodic self-sustained oscillations, it is effective for demonstrating the power of the mFVS control to readily achieve these oscillations.

Similar to the results from the FHN network (Fig. 1), in the HH network, periodic self-sustained oscillations arise and are encoded into the mFVS nodes. We find that different combinations of activated mFVS nodes lead to distinct oscillation patterns, as shown in Fig. 6 where, for $t < 800$ ms, the coupling strength of the activated mFVS node is $D = 0.1$ and the remaining mFVS nodes are suppressed. When the activated mFVS node is changed at $t = 800$ ms, as shown in Fig. 6(a), after a short transient time, the network settles down to a different attractor that depends on the specific activated neuron in mFVS, leading to distinct self-sustained oscillation patterns, as shown in Figs. 6(c)–6(e). The behavior of the inverse participation ratio $L$ of the power spectrum $S(T)$ is shown in Fig. 6(f), which is similar to that for the FHN network as in Fig. 2(c). When the mFVS nodes have a large coupling strength, e.g., $D > 0.07$, the oscillations become periodic with short periods as the network system now contains many short dynamical loops. For $D \lesssim 0.06$, chaotic oscillations arise, which are eventually unable to sustain themselves when all the mFVS nodes have been inhibited beyond the critical point $D_c \cong 0.015$, ruling out the existence of any loop.

## IV. DISCUSSION

Spatially distinct, self-sustained oscillations in excitable systems, such as ANN systems, are fundamental to information encoding, storage, and processing in these systems. An outstanding question is, what is the dynamical mechanism for an ANN to generate a large number of spatially distinct and robust self-sustained oscillations, each involving a different subset of neurons? We have addressed this question from the standpoint of complex nonlinear dynamical networks of excitable elements. Our main finding is that a variety of such oscillation patterns can be generated through exploiting a subset of special nodes in the network: nodes that belong to the mFVS—minimum feedback vertex set.[50,55,56] Particularly, an mFVS is a minimum set of nodes in the network whose removal (or

complete inhibition) will result in a tree-like, yet still mostly connected network without any loops. Our idea is then that activating or de-inhibiting some mFVS nodes would create some loops that can support periodic oscillations in a self-sustained manner. The present study has indeed revealed that this is the case: a variety of stable, self-sustained oscillation patterns can emerge through targeted activation of even a single mFVS node. While most results reported in this paper are for the case of exciting a single mFVS node, we find that de-inhibiting a subset of mFVS nodes can lead to a drastically richer variety of oscillation patterns. In the terminology of nonlinear dynamics, these patterns correspond to limit-cycle type of periodic attractors.

Another finding is that varying the coupling strength of the mFVS nodes with the remaining of the network continuously, e.g., by strengthening the inhibition level for all or some mFVS nodes, can drive the whole artificial neural network system into a chaotic attractor. We note that chaos can arise in ANNs with balanced excitatory and inhibitory activity.[64] The great advantage of chaos is that it can naturally facilitate switching among different self-sustained oscillation patterns. Particularly, suppose the current oscillation pattern becomes undesired. One can tune the inhibition level of the mFVS nodes so that the system settles into chaos, with which the activation of an mFVS node targeted at a different but desired oscillation pattern can drive the system quickly into the corresponding attractor. More generally, this implies the potential benefits of tuning the system near a critical state with chaos: there is great flexibility in achieving rapid switching among oscillation patterns depending on needs. In fact, there is belief that a healthy brain always works in a critical state (edge of chaos), where a rich variety of oscillation patterns exist.[65–67] While neural excitability generally depends on biological factors such as the inhibitory or excitatory synapse connections and the refractory period, these features of artificial neurons realized using circuits in a complex ANN can be readily regulated in a controllable way. Our work reveals a possible dynamical mechanism for generating and switching among such patterns—tasks that are essential for the normal functioning of the artificial neural networks.

It should be stressed that our controlling scheme captures the key ingredients, e.g., the background loop structure that supports the self-sustained oscillations, and do not depend on dynamical details. There are many neuronal systems that the synapses are based on chemical couplings, not the electrical couplings in this study. The main difference between chemical synapses and electrical synapses is their responses to subthreshold stimulus. For general electrical synapse models, different subthreshold stimulus can superimpose together naturally and activate the target neuron.[68] However, for chemical synapses, the response to subthreshold stimulus depends on details of models, e.g., short-term synaptic plasticity, which plays a significant role for chaotic oscillations.[69] For neuronal systems with chemical synapses, our results should still be valid as their self-sustained oscillations are again dominated by the loops, where the mFVS based controlling scheme will be efficient in modulating the oscillation patterns.

From an applied point of view, the finding that ANNs with complex connection topologies can generate a rich variety of spatially distinct, self-sustained oscillations through manipulation of a few or even a single mFVS node has applications in developing unconventional, non-Boolean type of computing paradigms for ANNs. Furthermore, our findings are robust against variations in the network topology, in system size, or in the neuronal dynamics of the nodes. Broad applications of our results could be expected in designing functional ANNs.

## ACKNOWLEDGMENTS

This work was partially supported by NSFC under Grant Nos. 11775101, 12175090, 11975178, and 12047501 and by the 111 Project under Grant No. B20063. Z.-G.H. acknowledges support of the K. C. Wong Education Foundation and the Natural Science Basic Research Plan in the Shaanxi Province of China (Program No. 2020JM-058). H.-J.Z. acknowledges support of the Chinese Academy of Sciences (Grant No. QYZDJ-SSW-SYS018). Y.-C.L. is supported by the Office of Naval Research through Grant No. N00014-21-1-2323 and by the Army Research Office through Grant No. W911NF-21-2-0055.

## AUTHOR DECLARATIONS

### Conflict of Interest

The authors have no conflicts to disclose.

## DATA AVAILABILITY

The data that support the findings of this study are available from the corresponding authors upon reasonable request.

## APPENDIX A: EFFECTS OF DIFFERENT NETWORK STRUCTURES OF ANNs

The results in the main text on exploiting mFVS for controlled generation of self-sustained oscillations in two types of ANNs are from regular random networks. Here, we demonstrate that the principle also holds for scale-free and small-world networks and is independent to the system sizes.

### 1. Scale-free networks

We generate three scale-free networks of size $N = 200$ and average degree $\langle k \rangle = 4$. For each network, we determine the FVS using $10^4$ independent runs using the algorithm in Ref. 50. As shown in Fig. 7(a), all FVS have size 21 so that the size of the mFVS is 21, which contains all hub nodes with degree larger than five. As the coupling strength $D$ of 20 nodes in the mFVS decreases, periodic oscillations of short periods, chaotic oscillations, and periodic oscillations of long periods, all self-sustained, emerge successively. Figure 7(b) shows the inverse participation ratio $L$ vs $D$. For either large or small values of $D$, in general, there are only one dominating oscillation pattern supported by a loop structure in the network, and the power spectrum concentrates on this period, leading to a large $L$ value. For $D \sim 0.1$, $L$ drops significantly, indicating a broad participation of many loops, whose competition results in the observed chaotic motion. This is similar to the results on regular random networks. Figure 7(c) further corroborates the above reasoning that, by inhibiting increasingly more neurons in the mFVS, the distribution of the periods becomes broader, signifying participation of the

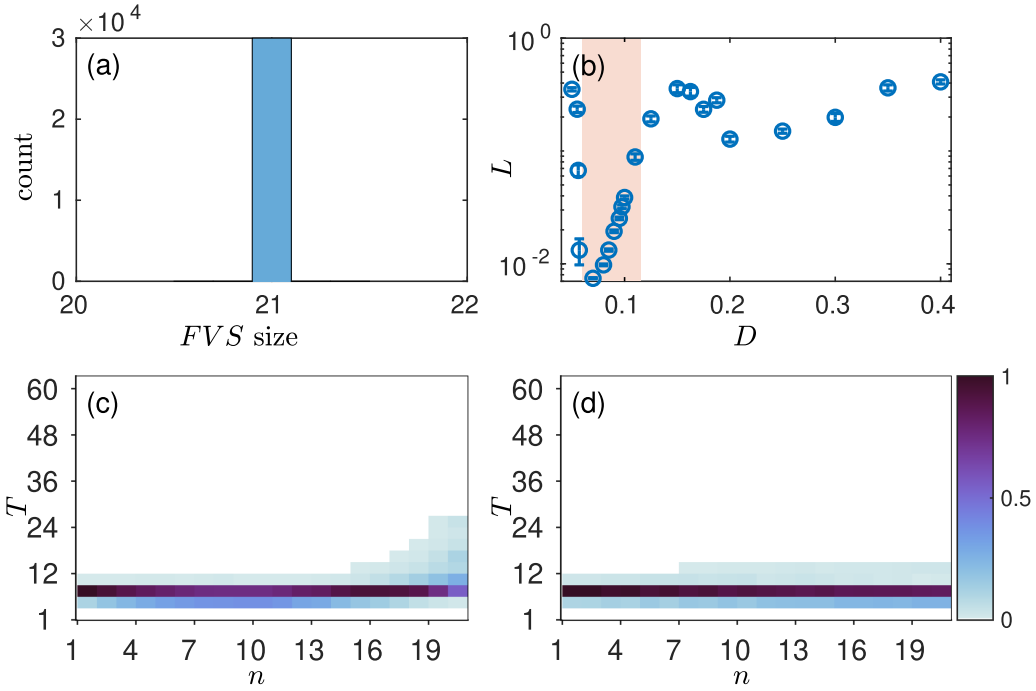


**FIG. 7.** Controlled generation of self-sustained oscillations in scale-free networks. The networks have size $N = 200$ and average degree $\langle k \rangle = 4$. (a) Size distribution of FVS. Three networks are generated, whose size of the mFVS is 21. For each network, the FVS is sampled from $10^4$ independent runs. (b) For one of the three networks, the inverse participation ratio $L$ of the power spectrum vs the coupling strength $D$. The shaded region with relatively small values of $L$ indicates broad participation of many dynamic loops in the network of varying periods, leading to chaotic oscillations. Each data point is obtained from 100 random initializations. (c) and (d) Distribution of the periods $T$ of sustained oscillations for inhibiting $n$ nodes in the mFVS and for randomly inhibiting $n$ nodes in the whole network, respectively. The maximum number of inhibited nodes $n$ is 20; i.e., only one node in the mFVS is not inhibited. For each $n$, the data are obtained from statistics of 1000 random initializations on each of the three networks.

different loop structures. In contrast, inhibiting randomly selected neurons in the whole system does not have such an effect, as shown in Fig. 7(d).

## 2. Small-world networks

Because of the refractory period of the neuron, a loop with four or fewer nodes cannot support self-sustained oscillations. However, one node in the loop must belong to the mFVS. To make a connection of the nodes in the mFVS with the self-sustained oscillation dynamics, we study a honeycomb lattice with periodic boundary conditions and random rewiring of 2% of the edge nodes to generate a small-world network, where the smallest loop has six nodes and so can support self-sustained oscillations. Figure 8(a) shows the distribution of the FVS size in three small-world networks of 224 nodes, indicating that the mFVS contains 59 nodes. As the coupling strength of the links between 58 nodes in mFVS and other nodes in the network decreases, the inverse participation ratio $L$ exhibits behaviors similar to those with regular random networks in the main text. Figure 8(b) shows $L$ vs $D$, where periodic oscillations of short periods occur in the region of relatively large $D$ values. As $D$ decreases from this region, chaotic oscillations arise. For $D < 0.09$, the controlled nodes have little response to their neighbors and periodic oscillations set in again. Figures 8(c) and 8(d) show the results of controlled and random generation of self-sustained oscillations, respectively. Similar to the results from regular-random networks in the main text and those with scale-free networks in Fig. 7, self-sustained oscillation patterns can be effectively generated by control.

## 3. Larger regular random networks

Here, we study larger regular random networks of size 400 and average degree $k = 3$. Figure 9(a) shows the distribution of the size of FVS. Three networks are chosen from several realizations whose mFVS contains 101 nodes. For each network, 10 000 runs of the FVS are obtained for statistical analysis. For the self-sustained oscillations, the inverse participation ratio $L$ of the power spectrum is calculated by inhibiting 100 nodes in the mFVS and leaving one node uncontrolled. Figure 9(b) shows $L$ vs $D$. A nearly plateaued region of $L$ values arises for $D > 0.2$, in which periodic self-sustained oscillations of short periods occur. As $D$ decreases from 0.2, $L$ drops suddenly and the oscillations become chaotic. When most of the mFVS nodes are inhibited, the remaining uncontrolled one or

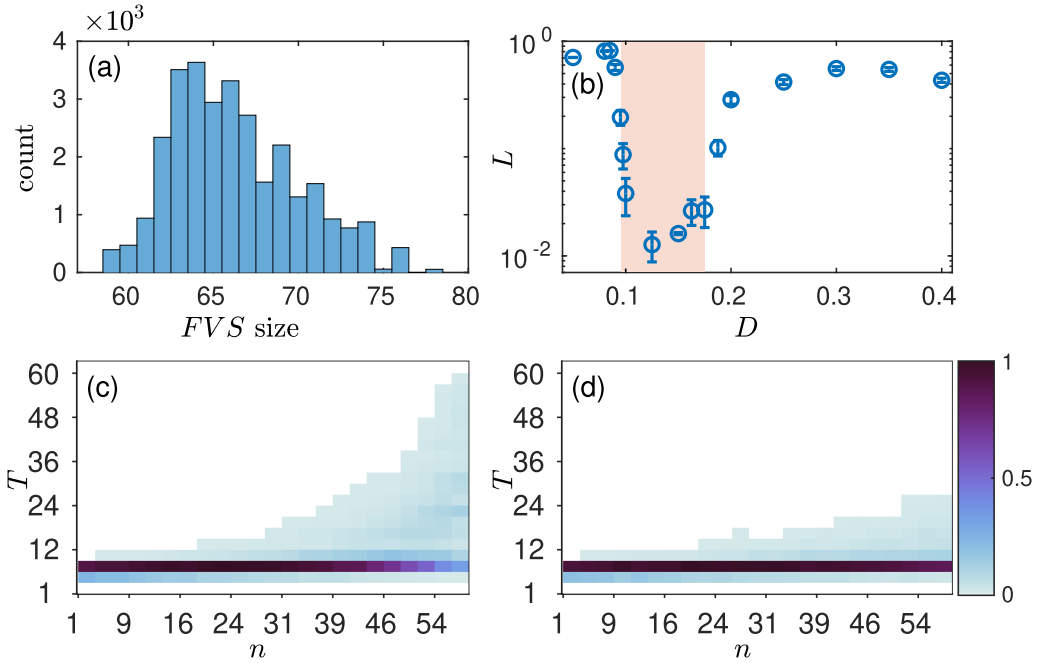


**FIG. 8.** The same plot as Fig. 7 but for small-world networks with $N = 224$ and $k = 3$. The size of the mFVS is 59.

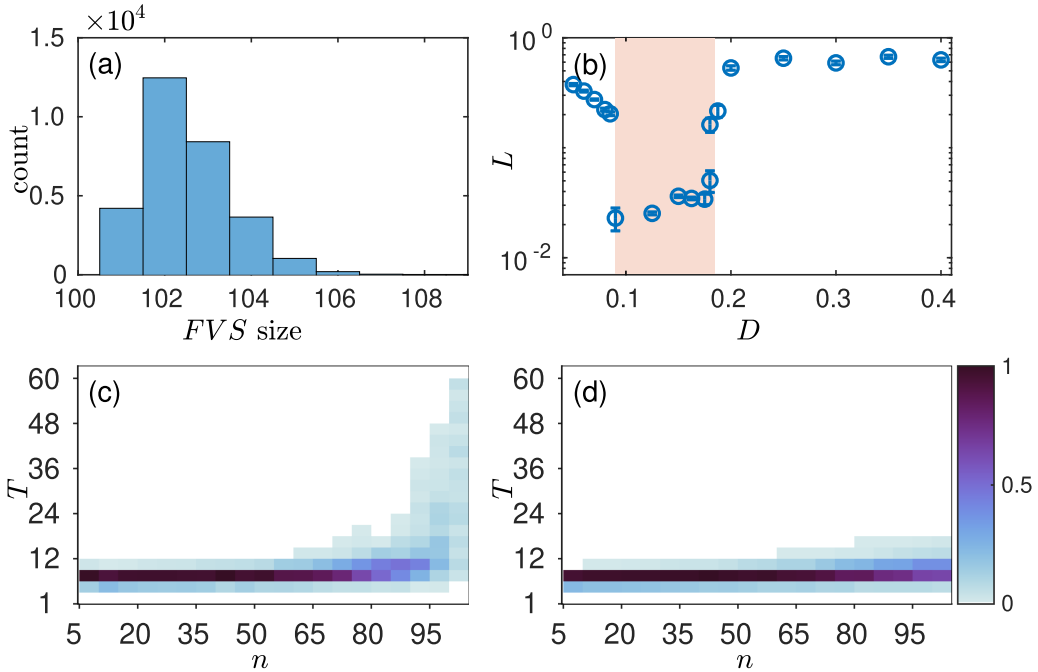


**FIG. 9.** The same plot as Fig. 7 but for larger regular random networks with $N = 400$ and $k = 3$. The size of the mFVS is 101.

two mFVS nodes lead to one or two loops that act as the "pacemaker" of the system. As a result, the number of distinct periods is reduced, leading to large $L$ values again and periodic oscillations of a long period. Controlling the nodes in the mFVS can significantly increase the period of oscillations and broaden the period distribution, as shown in Fig. 9(c). In contrast, inhibiting a set of randomly selected nodes from the whole system leads to a localized distribution, notwithstanding a small increase in the average period, as shown in Fig. 9(d).

## APPENDIX B: CONTROLLING LOOP STRUCTURES IN LARGER SYSTEMS BY mFVS

In the main text, we have shown that the dynamics of the FHN or HH networks are dominated by the loop structures, especially those of long periods in the neuronal activities. In general, the length of a loop that drives a self-sustained oscillation pattern is proportional to the oscillation period $T$. To demonstrate the effectiveness of the mFVS control on larger systems, instead of directly calculating the time evolution of the FHN system, we examine the

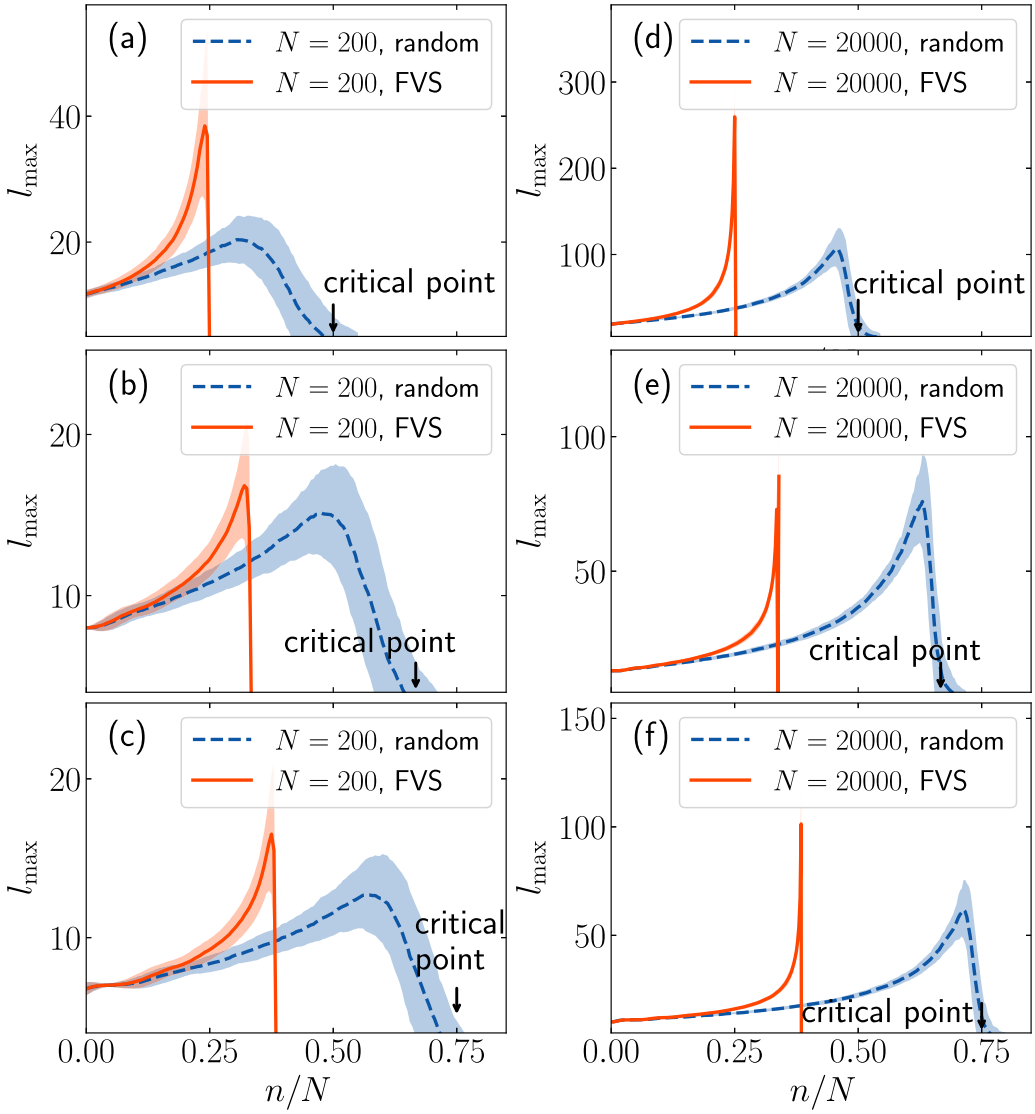


**FIG. 10.** Length of the longest loop after removing $n$ nodes vs $n/N$. The blue dashed and orange solid curves are the mean values for the cases of random removal and mFVS control (removing $n$ nodes belonging to the mFVS), respectively. For each parameter value around 500 realizations are carried out to obtain the mean and standard deviation, which is indicated by the shaded area around the mean value. The networks are of the regular random type with degree $k = 3$ for (a,d), $k = 4$ for (b,e) and $k = 5$ for (c,f). The system sizes are $N = 200$ for the left column, e.g., (a)–(c), and $N = 20\,000$ for the right column (d)–(f). The critical point of site percolation is marked by the black arrow.

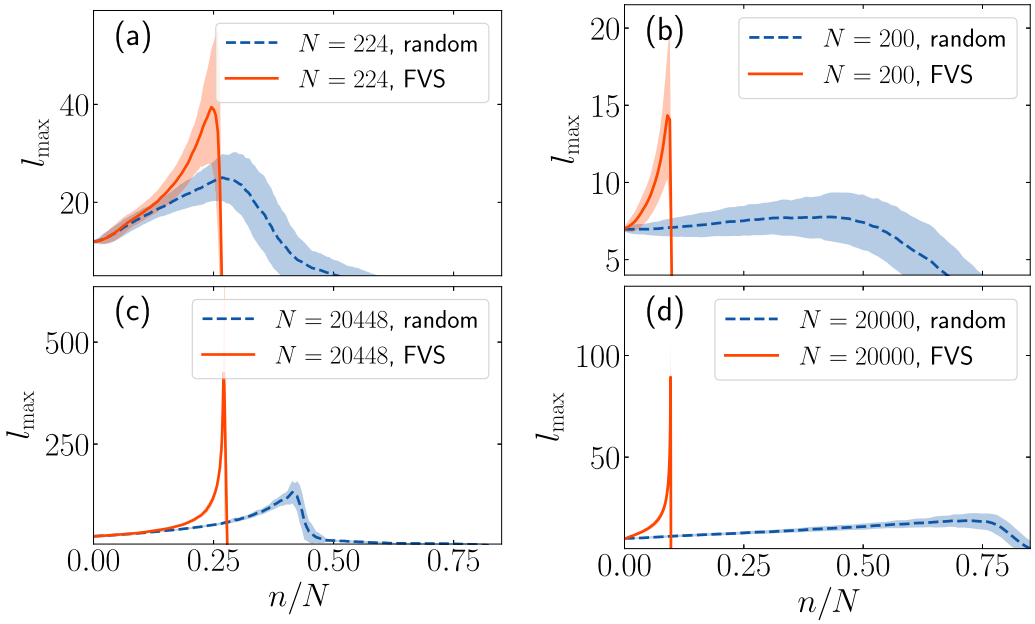


**FIG. 11.** The same plot as Fig. 10 but for small-world networks with $k = 3$ (a) and (c) and scale-free networks with $\langle k \rangle = 4$ (b) and (d). For these small-world networks, 2% of the edges are rewired to be long-range connections.

loop structures, especially those of the maximum length. Note that, for every pair of nodes in a loop, at least one path with the minimum length between them exists (the loop length). Only this kind of loops can serve as the "pacemaker" of the system and supports self-sustained oscillations. To be concrete, we examine, after removing $n$ nodes from the system, how the length of the longest loop $l_{\max}$ is changed. We compare two cases: (a) nodes are randomly removed from the mFVS and (b) nodes are removed randomly from the whole network, with the anticipation of the former scenario to have a more significant effect on $l_{\max}$.

Figure 10 demonstrates the average length of the longest loop for random control (blue dashed line) and mFVS control (orange solid line) for regular random networks of varying sizes and degrees, where the width of the shaded areas indicates the fluctuations of $l_{\max}$. Obviously, for larger networks, the relative deviation has much shrunk except at the critical point. Comparing with the distribution of the oscillation periods in Fig. 5 in the main text for $N = 200$ and that in Fig. 9(c) for $N = 400$, we find that the curves of $l_{\max}(n)$ are essentially identical to those oscillation periods obtained by solving the FHN dynamics.

The process of randomly inhibiting (removing) nodes until there is no loop in the network can be regarded as a site-percolation process. Since the size of the largest connected cluster is small when the fraction of inhibited nodes is beyond the critical point,[70,71] the longest length of the loop is restricted by the cluster size and will decrease abruptly about the critical point. As a result, the periods of the oscillation patterns are most abundant about the critical point, while the precise position of the peak of the distribution of the periods is affected by the finite-size effect. The black arrow in Fig. 10 marks the position of the critical point of site percolation, which is $n/N = (k-2)/(k-1)$ for infinite regular random networks. After site percolation occurs, large connected clusters no longer exist, neither do long loops. In contrast to random control, harnessing mFVS nodes can result in longer loops and make the generated self-sustained oscillations to achieve a longer period more efficiently, as fewer controlled nodes are needed. For larger degree $k$, a larger fraction of nodes need to be removed to reach the critical point. Figure 10 shows the results for $N = 200$ and $N = 20\,000$, while intermediate sizes have also been investigated. Comparing different network sizes, it has been found that the critical value of the mFVS control has little finite-size effects, indicating that the size of mFVS is proportional to the system size. Similar results have been obtained for two-dimensional small-world networks with $k = 3$ and scale-free networks with $\langle k \rangle = 4$ (Fig. 11). These results provide further support for the conclusion in the main text, with generalization to networked systems of larger sizes, of different connection density, and of different types of topology.

## REFERENCES

[1] E. Goto, "New parametron circuit element using nonlinear reactance," KDD Kenyku Shiryo, 1954.
[2] J. von Neumann, "Non-linear capacitance or inductance switching, amplifying, and memory organs," U.S. patent US2815488 (3 December 1957).
[3] R. A. Kiehl and T. Ohshima, "Bistable locking of single-electron tunneling elements for digital circuitry," Appl. Phys. Lett. **67**, 2494–2496 (1995).
[4] T. Ohshima and R. A. Kiehl, "Operation of bistable phase-locked single-electron tunneling logic elements," J. Appl. Phys. **80**, 912–923 (1996).

[5]E. M. Izhikevich, "Weakly pulse-coupled oscillators, FM interactions, synchronization, and oscillatory associative memory," IEEE Trans. Neural Networks **10**, 508–526 (1999).
[6]T. Yang, R. A. Kiehl, and L. O. Chua, "Tunneling phase logic cellular nonlinear networks," Int. J. Bifurcation Chaos **11**, 2895–2911 (2001).
[7]T. Li and R. Kiehl, "Operating regimes for multivalued single-electron tunneling phase logic," J. Appl. Phys. **93**, 9291–9297 (2003).
[8]N. A. Nezlobin and R. A. Kiehl, "Phase-locking in a nonuniform array of tunnel junctions," J. Appl. Phys. **94**, 6841–6848 (2003).
[9]T. Nishikawa, Y.-C. Lai, and F. C. Hoppensteadt, "Capacity of oscillatory associative-memory networks with error-free retrieval," Phys. Rev. Lett. **92**, 108101 (2004).
[10]T. Nishikawa, F. C. Hoppensteadtb, and Y.-C. Lai, "Oscillatory associative memory network with perfect retrieval," Physica D **197**, 134–148 (2004).
[11]R. A. Kiehl, "Information processing by nonlinear phase dynamics in locally connected arrays," arXiv:1603.06665 (2016).
[12]C.-Z. Wang, H.-Y. Xu, N. D. Rizzo, R. A. Kiehl, and Y.-C. Lai, "Phase locking of a pair of ferromagnetic nano-oscillators on a topological insulator," Phys. Rev. Appl. **10**, 064003 (2018).
[13]L. Glass and M. C. Mackey, *From Clocks to Chaos: The Rhythms of Life* (Princeton University Press, Princeton, NJ, 1988).
[14]M. C. Mackey and L. Glass, "Oscillation and chaos in physiological control systems," Science **197**, 287–289 (1977).
[15]L. Glass, "Synchronization and rhythmic processes in physiology," Nature **410**, 277–284 (2001).
[16]X.-J. Wang, "Neurophysiological and computational principles of cortical rhythms in cognition," Physiol. Rev. **90**, 1195–1268 (2010).
[17]R. Stoop, V. Saase, C. Wagner, B. Stoop, and R. Stoop, "Beyond scale-free small-world networks: Cortical columns for quick brains," Phys. Rev. Lett. **110**, 108105 (2013).
[18]K. Kanders, H. Lee, N. Hong, Y. Nam, and R. Stoop, "Fingerprints of a second order critical line in developing neural networks," Commun. Phys. **3**, 13 (2020).
[19]X.-J. Wang, H. Hu, C. Huang, H. Kennedy, C. T. Li, N. Logothetis, Z.-L. Lu, Q. Luo, M.-M. Poo, D. Tsao, S. Wu, Z. Wu, X. Zhang, and D. Zhou, "Computational neuroscience: A frontier of the 21st century," Natl. Sci. Rev. **7**, 1418–1422 (2020).
[20]B. Romeira, J. M. Figueiredo, and J. Jvaloyes, "Delay dynamics of neuromorphic optoelectronic nanoscale resonators: Perspectives and applications," Chaos **27**, 114323 (2017).
[21]M. Kuperman and G. Abramson, "Small world effect in an epidemiological model," Phys. Rev. Lett. **86**, 2909 (2001).
[22]R. Pastor-Satorras and A. Vespignani, "Epidemic spreading in scale-free networks," Phys. Rev. Lett. **86**, 3200 (2001).
[23]M. Tinsley, J. Cui, F. V. Chirila, A. Taylor, S. Zhong, and K. Showalter, "Spatiotemporal networks in addressable excitable media," Phys. Rev. Lett. **95**, 038306 (2005).
[24]A. T. Winfree and J. J. Tyson, "When time breaks down: The three-dimensional dynamics of electrochemical waves and cardiac arrhythmias," Phys. Today **41**(12), 107 (1988).
[25]O. Sporns, D. R. Chialvo, M. Kaiser, and C. C. Hilgetag, "Organization, development and function of complex brain networks," Trends Cogn. Sci. **8**, 418–425 (2004).
[26]M. Müller-Linow, C. C. Hilgetag, and M.-T. Hütt, "Organization of excitable dynamics in hierarchical biological networks," PLoS Comput. Biol. **4**, e1000190 (2008).
[27]A. Roxin, H. Riecke, and S. A. Solla, "Self-sustained activity in a small-world network of excitable neurons," Phys. Rev. Lett. **92**, 198101 (2004).
[28]S. Sinha, J. Saramäki, and K. Kaski, "Emergence of self-sustained patterns in small-world excitable media," Phys. Rev. E **76**, 015101 (2007).
[29]C. M. Gray, "Synchronous oscillations in neuronal systems: Mechanisms and functions," J. Comput. Neurosci. **1**, 11–38 (1994).
[30]G. Buzsáki and A. Draguhn, "Neuronal oscillations in cortical networks," Science **304**, 1926–1929 (2004).
[31]W. M. Usrey and R. C. Reid, "Synchronous activity in the visual system," Annu. Rev. Physiol. **61**, 435–456 (1999).
[32]L. M. Ward, "Synchronous neural oscillations and cognitive processes," Trends Cogn. Sci. **7**, 553–559 (2003).
[33]M. Stopfer, S. Bhagavan, B. H. Smith, and G. Laurent, "Impaired odour discrimination on desynchronization of odour-encoding neural assemblies," Nature **390**, 70–74 (1997).
[34]M. Steriade, D. A. McCormick, and T. J. Sejnowski, "Thalamocortical oscillations in the sleeping and aroused brain," Science **262**, 679–685 (1993).
[35]T. J. Lewis and J. Rinzel, "Self-organized synchronous oscillations in a network of excitable cells coupled by gap junctions," Netw. Comput. Neural Syst. **11**, 299–320 (2000).
[36]A. J. Steele, M. Tinsley, and K. Showalter, "Spatiotemporal dynamics of networks of excitable nodes," Chaos **16**, 015110 (2006).
[37]R. FitzHugh, "Impulses and physiological states in theoretical models of nerve membrane," Biophys. J. **1**, 445–466 (1961).
[38]T. Lilienkamp, J. Christoph, and U. Parlitz, "Features of chaotic transients in excitable media governed by spiral and scroll waves," Phys. Rev. Lett. **119**, 054101 (2017).
[39]T. Lilienkamp and U. Parlitz, "Terminal transient phase of chaotic transients," Phys. Rev. Lett. **120**, 094101 (2018).
[40]J. M. Fuster, *Memory in the Cerebral Cortex* (MIT Press, Cambridge, MA, 1995).
[41]D. Durstewitz, J. K. Seamans, and T. J. Sejnowski, "Neurocomputational models of working memory," Nat. Neurosci. **3**, 1184–1191 (2000).
[42]P. S. Goldman-Rakic, S. Funahashi, and C. J. Bruce, "Neocortical memory circuits," Cold Spring Harb. Symp. Quant. Biol. **55**, 1025 (1990).
[43]M. Goldman, F. Koester, K. Luedge, and S. Yanchuk, "Deep time-delay reservoir computing: Dynamics and memory capacity," Chaos **30**, 093124 (2020).
[44]A. Zeng, Y.-Q. Hu, and Z.-R. Di, "Unevenness of loop location in complex networks," Phys. Rev. E **81**, 046121 (2010).
[45]X. Ma, L. Huang, Y.-C. Lai, and Z. Zheng, "Emergence of loop structure in scale-free networks and dynamical consequences," Phys. Rev. E **79**, 056106 (2009).
[46]G. Bianconi and A. Capocci, "Number of loops of size $h$ in growing scale-free networks," Phys. Rev. Lett. **90**, 078701 (2003).
[47]G. Bianconi, N. Gulbahce, and A. E. Motter, "Local structure of directed networks," Phys. Rev. Lett. **100**, 118701 (2008).
[48]X.-H. Liao, Q.-Z. Xia, Y. Qian, L.-S. Zhang, G. Hu, and Y.-Y. Mi, "Pattern formation in oscillatory complex networks consisting of excitable nodes," Phys. Rev. E **83**, 056204 (2011).
[49]Y.-Y. Mi, X.-H. Liao, X.-H. Huang, L.-S. Zhang, W.-F. Gu, G. Hu, and S. Wu, "Long-period rhythmic synchronous firing in a scale-free network," Proc. Natl. Acad. Sci. U.S.A. **110**, E4931–E4936 (2013).
[50]H.-J. Zhou, "Spin glass approach to the feedback vertex set problem," Euro. Phys. J. B **86**, 455 (2013).
[51]S. Mugisha and H.-J. Zhou, "Identifying optimal targets of network attack by belief propagation," Phys. Rev. E **94**, 012305 (2016).
[52]J.-H. Zhao and H.-J. Zhou, "Statistical physics of hard combinatorial optimization: Vertex cover problem," Chin. Phys. B **23**, 078901 (2014).
[53]F. Morone and H. Makse, "Influence maximization in complex networks through optimal percolation," Nature **524**, 65–68 (2015).
[54]S.-M. Qin, "Spin-glass model for the $c$-dismantling problem," Phys. Rev. E **98**, 062309 (2018).
[55]B. Fiedler, A. Mochizuki, G. Kurosawa, and D. Saito, "Dynamics and control at feedback vertex sets I: Informative and determining nodes in regulatory networks," J. Dyn. Differ. Equ. **25**, 563–604 (2013).
[56]A. Mochizuki, B. Fiedler, G. Kurosawa, and D. Saito, "Dynamics and control at feedback vertex sets II: A faithful monitor to determine the diversity of molecular activities in regulatory networks," J. Theor. Biol. **335**, 130–146 (2013).
[57]M. Bär and M. Eiswirth, "Turbulence due to spiral breakup in a continuous excitable medium," Phys. Rev. E **48**, R1635–R1637 (1993).
[58]J. Nagumo, S. Arimoto, and S. Yoshizawa, "An active pulse transmission line simulating nerve axon," Proc. IRE **50**, 2061–2070 (1962).
[59]A. L. Hodgkin and A. F. Huxley, "A quantitative description of membrane current and its application to conduction and excitation in nerve," J. Physiol. **17**, 500–544 (1952).
[60]M. Uzuntarla, "Firing dynamics in hybrid coupled populations of bistable neurons," Neurocomputing **367**, 328–336 (2019).
[61]E. Ott, C. Grebogi, and J. A. Yorke, "Controlling chaos," Phys. Rev. Lett. **64**, 1196–1199 (1990).

[62]C. Grebogi and Y.-C. Lai, "Controlling chaos in high dimensions," IEEE Trans. Circuits Syst. I **44**, 971–975 (1997).
[63]C. Grebogi and Y.-C. Lai, "Controlling chaotic dynamical systems," Syst. Control Lett. **31**, 307–312 (1997).
[64]C. van Vreeswijk and H. Sompolinsky, "Chaos in neuronal networks with balanced excitatory and inhibitory activity," Science **274**, 1724–1726 (1996).
[65]O. Kinouchi and M. Copelli, "Optimal dynamical range of excitable networks at criticality," Nat. Phys. **2**, 348–351 (2006).
[66]N. Friedman, S. Ito, B. A. Brinkman, M. Shimono, R. L. DeVille, K. A. Dahmen, J. M. Beggs, and T. C. Butler, "Universal critical dynamics in high resolution neuronal avalanche data," Phys. Rev. Lett. **108**, 208102 (2012).
[67]A. Haimovici, E. Tagliazucchi, P. Balenzuela, and D. R. Chialvo, "Brain organization into resting state networks emerges at criticality on a model of the human connectome," Phys. Rev. Lett. **110**, 178101 (2013).
[68]P. Alcamí and A. E. Pereda, "Beyond plasticity: The dynamic impact of electrical synapses on neural circuits," Nat. Rev. Neurosci. **20**, 253–271 (2019).
[69]R. Zeraati, V. Priesemann, and A. Levina, "Self-organization toward criticality by synaptic plasticity," Front. Phys. **9**, 619661 (2021).
[70]J.-Q. Dong, Z. Shen, Y. Zhang, Z.-G. Huang, L. Huang, and X.-S. Chen, "Finite-size scaling of clique percolation on two-dimensional moore lattices," Phys. Rev. E **97**, 052133 (2018).
[71]M.-X. Liu, J.-F. Fan, L.-S. Li, and X.-S. Chen, "Continuous percolation phase transitions of two-dimensional lattice networks under a generalized Achlioptas process," Eur. Phys. J. B **85**, 132 (2012).